Electronic Supplementary Information (ESI)

Effective Hole and Electron Transport in Solution-Processable Nanoscale Films of a Deep-Green Dye exhibiting Room-Temperature Columnar Mesophases

Ritobrata De,[‡a] Joydip De,[‡a] Alvin Joseph,[b] Santosh Prasad Gupta,[c] Manoj A. G. Namboothiry*[b] and Santanu Kumar Pal*[a]

[a]*Department of Chemical Sciences, Indian Institute of Science Education and Research (IISER) Mohali, Sector-81, SAS Nagar, Knowledge City, Manauli 140306, India.*

[b]*School of Physics, Indian Institute of Science Education and Research (IISER) Thiruvananthapuram, 695 551 Kerala, India.*

[c]*Department of Physics, Patna University, Patna, Bihar 800005, India.*

E-mail: skpal@iisermohali.ac.in, manoj@iisertvm.ac.in

[‡]These authors contributed equally

Table of Contents

1) Materials and Methods S2
2) Synthesis and characterization S2
3) NMR Spectra: S4
4) Mass Spectra: S10
5) POM Studies: S11
6) DSC Thermograms: S11
7) TGA Curves: S11
8) X-ray Scattering Studies: S12
9) Photophysical Studies: S17
10) Electrochemical Studies: S17
11) Computational Studies: S17
12) Nanofilm and charge transport studies: S18
13) References: S20

1) Materials and Methods

Materials. Chemicals and solvents (AR quality) were used as received without any further purification. Column chromatographic separations were performed on silica gel (100-200 & 60-120 mesh). Thin layer chromatography (TLC) was performed on aluminium sheets pre-coated with silica gel (Merck, Kieselgel 60, F254).

Measurements and Characterization. *The detailed specifications of instruments used for the characterization of the synthesized compounds, including NMR, Mass and IR spectroscopy, Polarized Optical Microscopy (POM), Thermogravimetric analysis (TGA), Differential Scanning Calorimetry (DSC), X-Ray diffraction (XRD), photophysical studies (UV-Vis), electrochemical characterization (Cyclic voltammetry) are similar as mentioned in earlier reports from our group.[1] Laurell WS-650MZ-23NPP Spin-coater was used for fabrication of thin films. The I-V characteristic measurements were carried out with a Keithley 6430 source meter unit. Dielectric constants were measured using Agilent E4980A LCR meter, and the AC signal amplitude was 20 mV.*

2) Synthesis and characterization

The synthesis of **OXDANT** DLCs was carried out in our prior work as precursors to the final compound.[1] The synthetic procedures and the numerical ^{1}H NMR and ^{13}C NMR data are completely identical with those reported in the previous reference paper. For the readers' convenience, a re-outlined schematic is shown below, and the numerical ^{1}H NMR and ^{13}C NMR data are reproduced from the reference.[1] In addition to the numerical NMR data, the NMR spectra are added, along with ATR-IR and MALDI-MS data for the **OXDANT** DLCs.

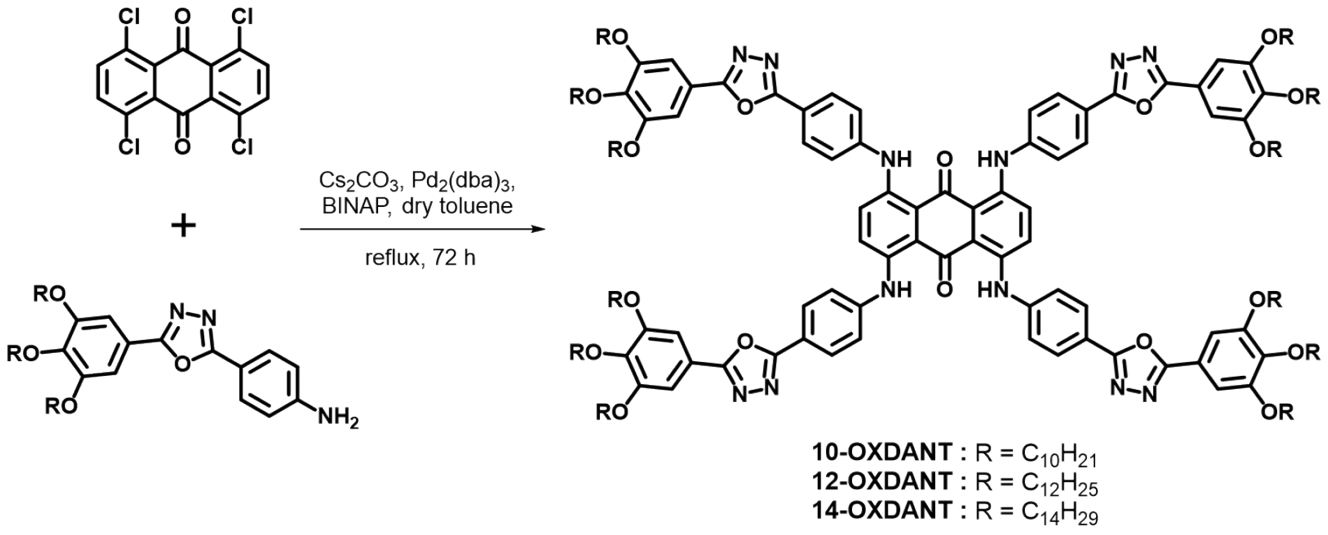

10-OXDANT : R = $C_{10}H_{21}$
12-OXDANT : R = $C_{12}H_{25}$
14-OXDANT : R = $C_{14}H_{29}$

1,4,5,8-tetrakis((4-(5-(3,4,5-tris(decyloxy)phenyl)-1,3,4-oxadiazol-2-yl)phenyl)amino)anthracene-9,10-dione (10-OXDANT):

^{1}H NMR (400 MHz, $CDCl_3$, δ ppm): 11.91 (s, 4H), 8.14 (d, J = 8Hz, 8H), 7.75 (s, 4H), 7.44 (d, J = 8Hz, 8H), 7.31 (s, 8H), 4.14-4.00 (m, 24H), 1.90-1.71 (m, 24H), 1.55-1.43 (m, 24H), 1.42-1.20 (m, 144H), 0.92-0.81 (m, 36H).

^{13}C NMR (100 MHz, $CDCl_3$, δ ppm):164.55, 164.17, 153.69, 143.62, 141.43, 140.70, 128.50, 121.43, 118.62, 105.44, 73.73, 69.48, 32.07, 32.04, 30.48, 29.88, 29.81, 29.78, 29.73, 29.56, 29.53, 29.49, 26.24, 26.22, 22.83, 22.81, 14.24.

ATR-IR (ν/cm^{-1}): 2923.7, 2853.6, 1729.4, 1599.1, 1557.1, 1491.8, 1431.9, 1362.4, 1327.6, 1258.6, 1210.2, 1179.4, 1117.0, 1010.5, 980.9, 807.5, 738.2, 716.8.

MALDI-MS: *m/z* calcd for $C_{190}H_{284}N_{12}O_{18}$ $(M+H)^+$: 3024.1744. Found: 3024.5820.

1,4,5,8-tetrakis((4-(5-(3,4,5-tris(dodecyloxy)phenyl)-1,3,4-oxadiazol-2-yl)phenyl)amino)anthracene-9,10-dione (12-OXDANT):

^{1}H NMR (400 MHz, $CDCl_3$, δ ppm): 11.92 (s, 4H), 8.13 (d, J = 8Hz, 8H), 7.73 (s, 4H), 7.42 (d, J = 8Hz, 8H), 7.30 (s, 8H), 4.12-3.98 (m, 24H), 1.92-1.70 (m, 24H), 1.55-1.44 (m, 24H), 1.42-1.14 (m, 192H), 0.92-0.80 (m, 36H).

^{13}C NMR (100 MHz, $CDCl_3$, δ ppm): 164.61, 164.24, 153.74, 143.74, 141.48, 140.80, 128.58, 124.20, 121.54, 118.68, 118.66, 116.15, 105.53, 73.78, 69.54, 37.24, 35.00, 34.66, 32.09, 32.07, 31.57, 30.50, 30.32, 29.90, 29.85, 29.80, 29.74, 29.57, 29.55, 29.51, 29.49, 26.26, 26.23, 22.84, 14.27.

ATR-IR (ν/cm^{-1}): 2918.3, 2853.9, 1737.4, 1595.8, 1555.0, 1491.6, 1435.6, 1364.6, 1325.6, 1255.6, 1209.9, 1179.8, 1113.4, 1012.2, 976.8, 824.6, 738.2, 718.4.

MALDI-MS: *m/z* calcd for $C_{214}H_{332}N_{12}O_{18}$ $(M+H)^+$: 3360.5500. Found: 3360.5525.

1,4,5,8-tetrakis((4-(5-(3,4,5-tris(tetradecyloxy)phenyl)-1,3,4-oxadiazol-2-yl)phenyl)amino)anthracene-9,10-dione (14-OXDANT):

^{1}H NMR (400 MHz, $CDCl_3$, δ ppm): 11.92 (s, 4H), 8.14 (d, J = 8Hz, 8H), 7.75 (s, 4H), 7.44 (d, J = 8Hz, 8H), 7.31 (s, 8H), 4.12-3.98 (m, 24H), 1.92-1.70 (m, 24H), 1.55-1.44 (m, 24H), 1.42-1.14 (m, 240H), 0.92-0.80 (m, 36H).

^{13}C NMR (100 MHz, $CDCl_3$, δ ppm): 186.52, 164.60, 164.24, 153.73, 143.72, 141.47, 140.80, 139.42, 128.57, 124.19, 121.54, 118.67, 118.65, 116.14, 105.51, 73.78, 69.54, 33.97, 32.07, 30.50, 30.43, 29.90, 29.86, 29.84, 29.80, 29.74, 29.57, 29.54, 29.51, 29.49, 29.30, 29.09, 26.26, 26.24, 22.84, 14.27.

ATR-IR (ν/cm^{-1}): 2922.7, 2849.0, 1731.4, 1594.1, 1556.3, 1491.8, 1436.2, 1361.2, 1326.6, 1258.6, 1208.2, 1178.4, 1114.0, 1011.8, 977.3, 819.4, 739.7, 716.5.

MALDI-MS: *m/z* calcd for $C_{238}H_{380}N_{12}O_{18}$ $(M+H)^+$: 3696.9256 Found: 3696.8096.

3) NMR Spectra:

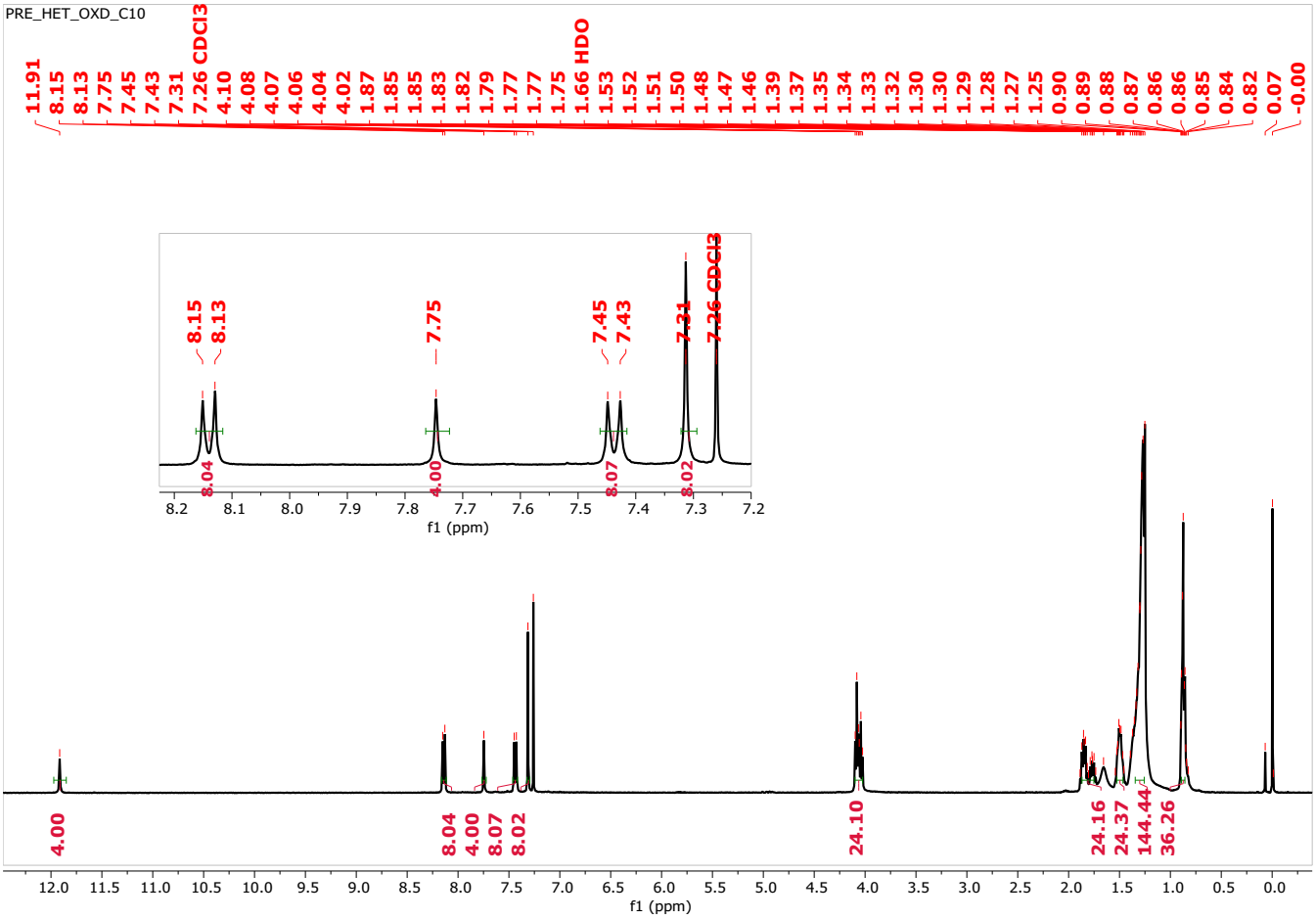

Fig. S1 ^{1}H NMR of **10-OXDANT** (400 MHz, $CDCl_3$).

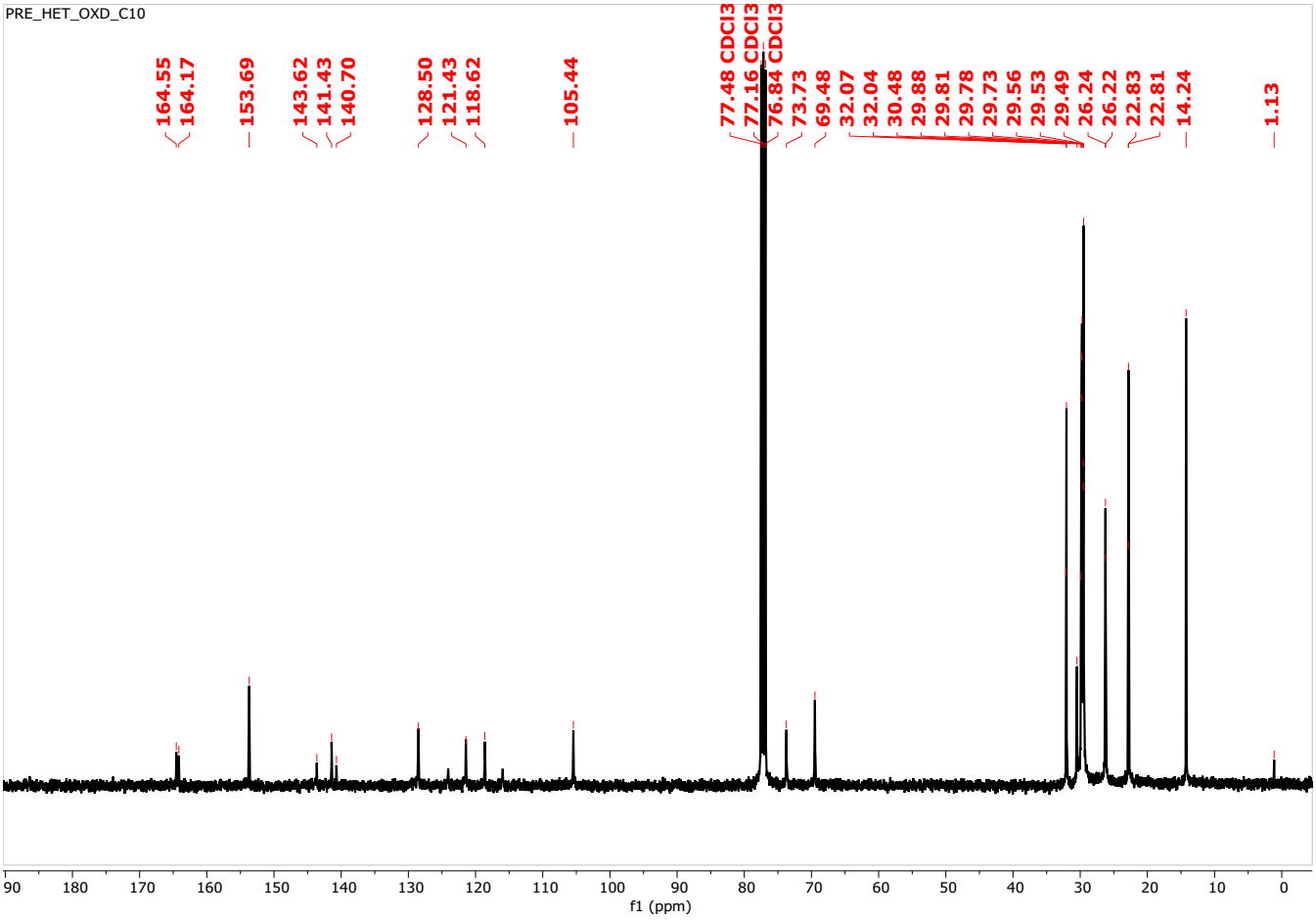

Fig. S2 ^{13}C NMR of **10-OXDANT** (100 MHz, $CDCl_3$).

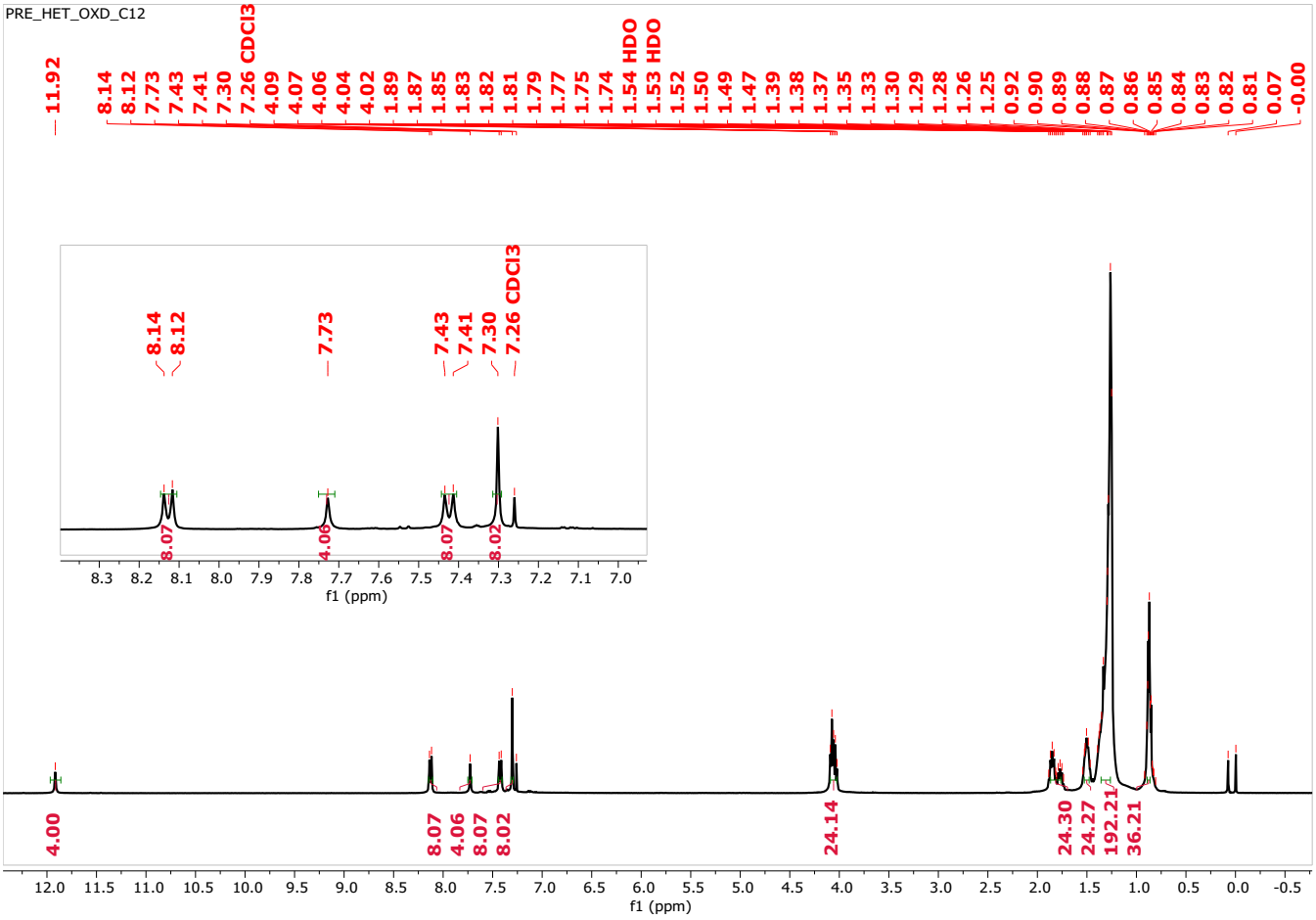

Fig. S3 ^{1}H NMR of **12-OXDANT** (400 MHz, $CDCl_3$).

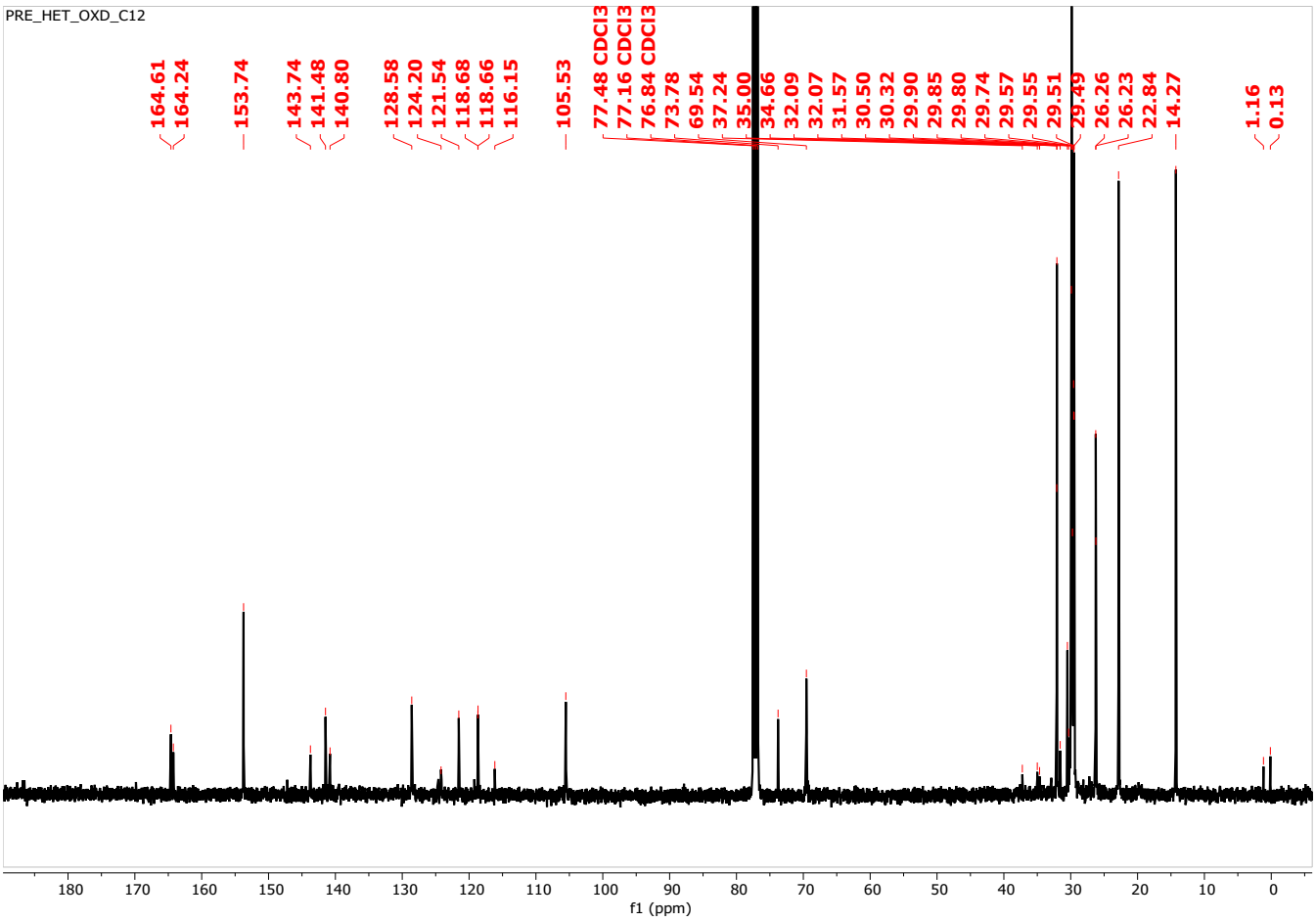

Fig. S4 ^{13}C NMR of **12-OXDANT** (100 MHz, $CDCl_3$).

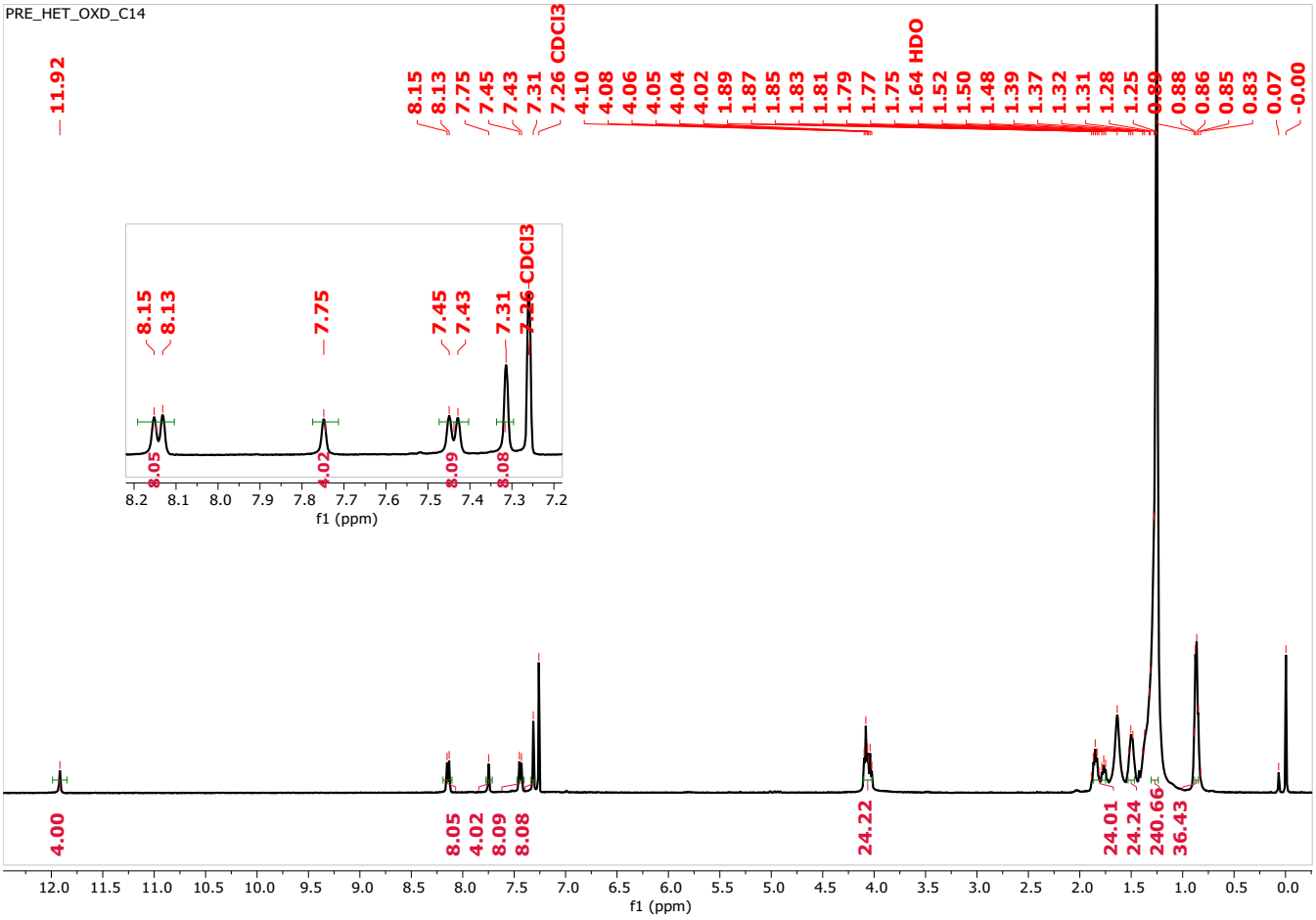

Fig. S5 ^{1}H NMR of **14-OXDANT** (400 MHz, $CDCl_3$).

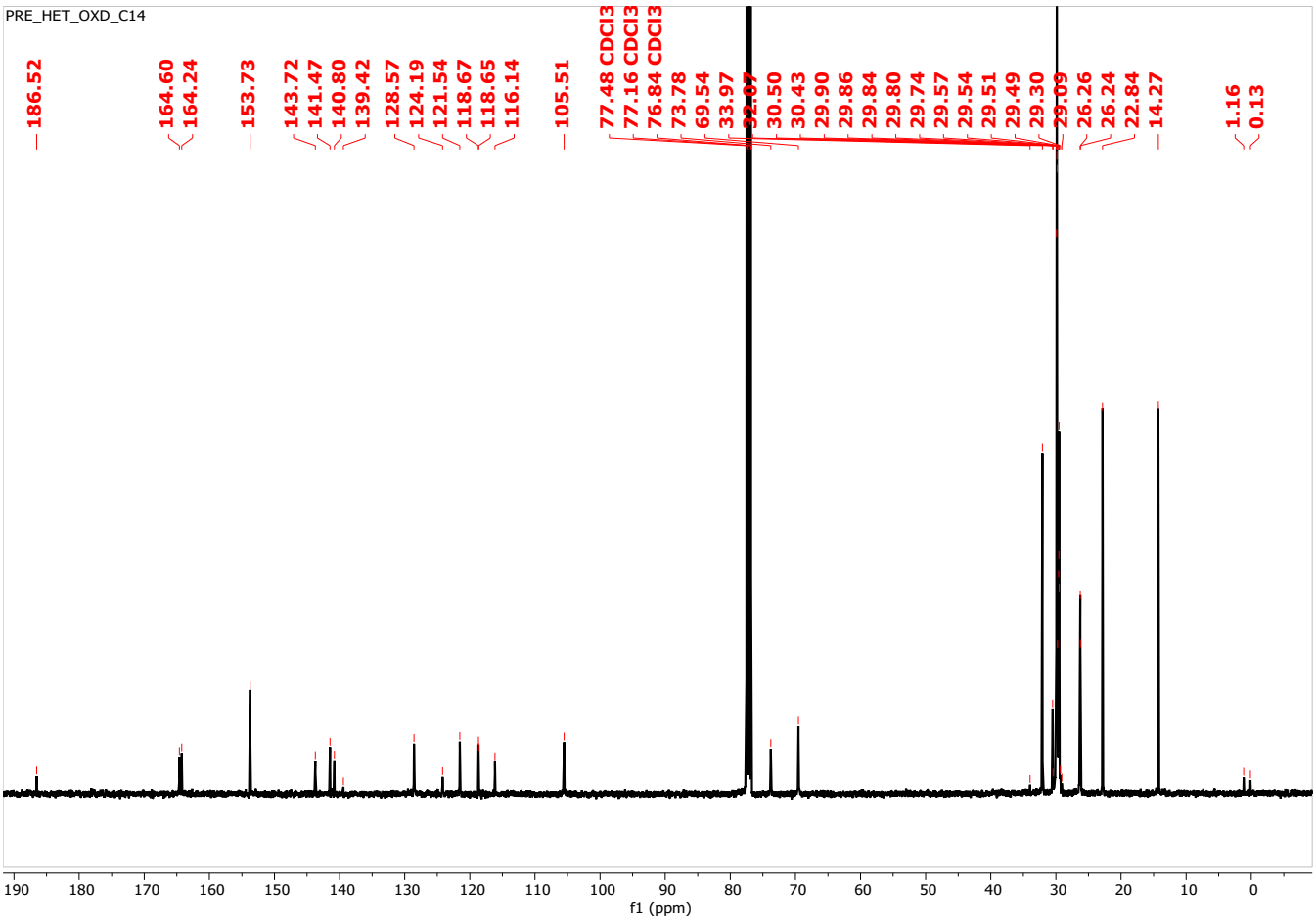

Fig. S6 ^{13}C NMR of **14-OXDANT** (100 MHz, $CDCl_3$).

4) Mass Spectra:

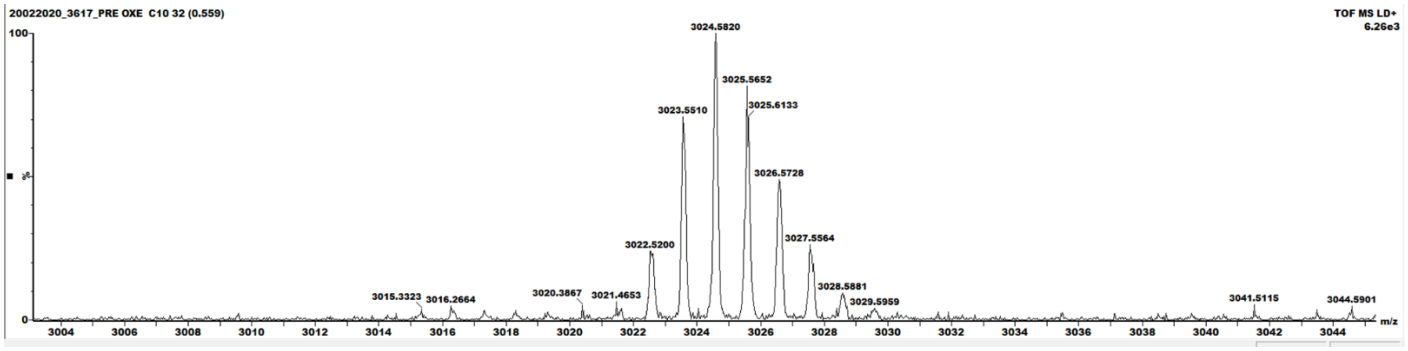

Fig. S7 MALDI-MS spectrum of **10-OXDANT**.

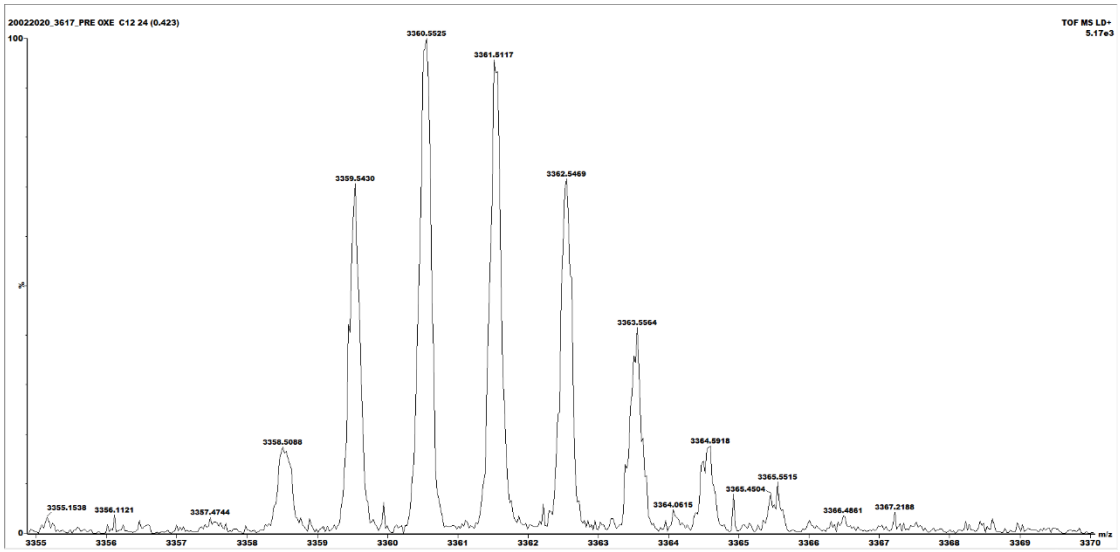

Fig. S8 MALDI-MS spectrum of **12-OXDANT**.

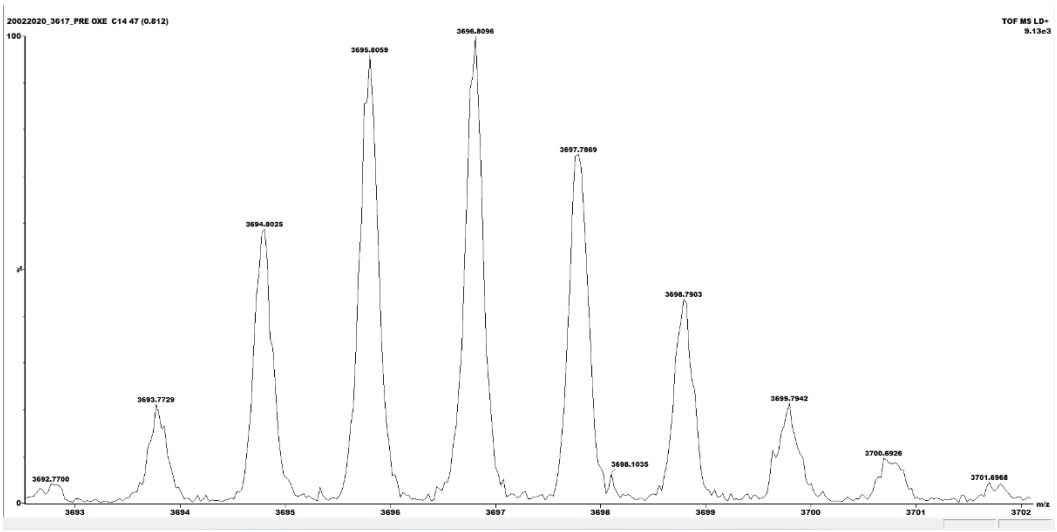

Fig. S9 MALDI-MS spectrum of **14-OXDANT**.

5) POM Studies:

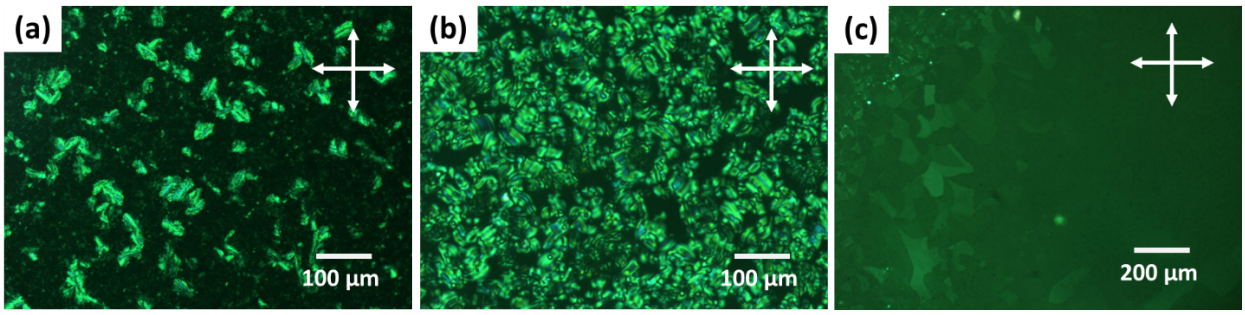

Fig. S10 POM images of (a) **10-OXDANT** at 181.5 °C, (b) **12-OXDANT** at 152.7 °C, and (c) **14-OXDANT** at 145.6 °C, on cooling from isotropic liquid kept between a glass slide and coverslip (polydomain orientations and averaging effects governing the effective optical retardation in certain regimes give rise to the low birefringent regions).

6) DSC Thermograms:

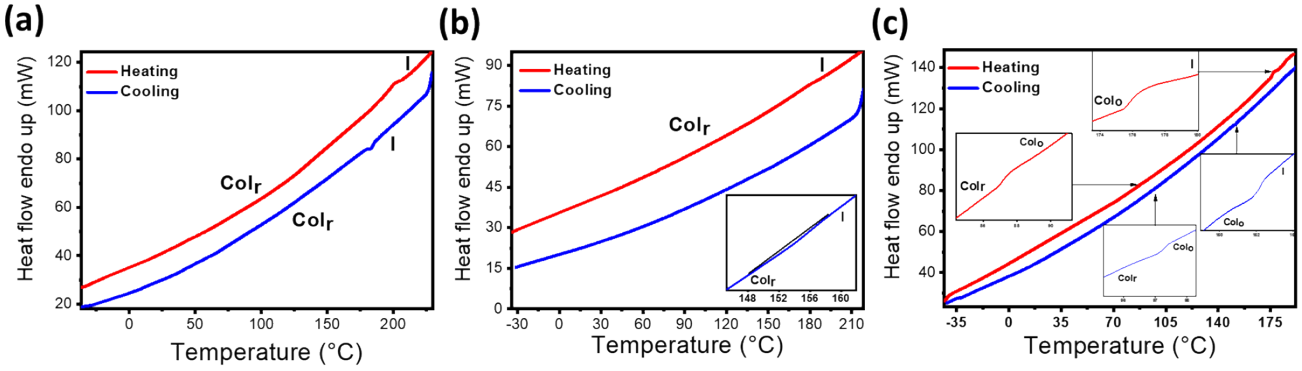

F ig. S11 DSC thermograms of compound (a) **10-OXDANT,** (b) **12-OXDANT** and (c) **14-OXDANT** at heating and cooling rates of 10 °C/min (recorded for the second heating and second cooling cycles), with the phase-transition regions magnified. Abbreviations: Col_r = Columnar rectangular, Col_o = Columnar oblique, I = Isotropic liquid.

7) TGA Curves:

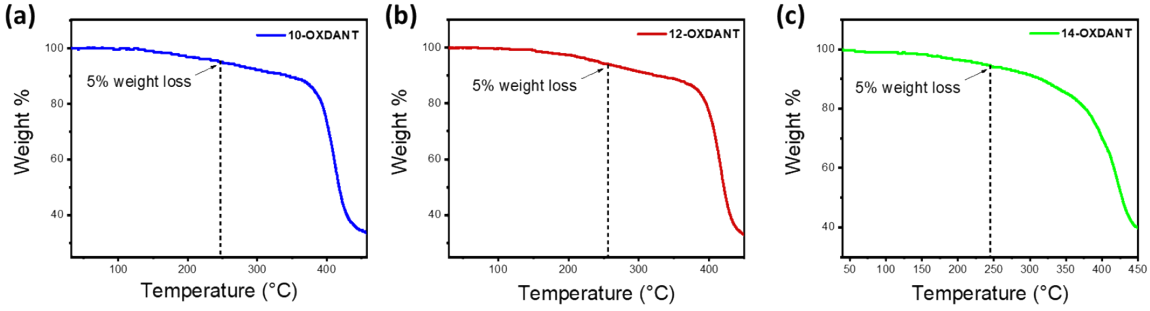

Fig. S12 TGA curves of (a) **10-OXDANT,** (b) **12-OXDANT** and (c) **14-OXDANT**. The measurements were performed under a nitrogen atmosphere, with a heating rate of 10 °C/min.

Table S1. Experimental data of thermal properties of **OXDANT** DLCs.[a,b]

DLC	Heating Scan	Cooling Scan	Decomposition (°C) from TGA
10-OXDANT	Col_r 200.4 (1.75) I[a]	I 183.1 (5.33) Col_r[a]	249
12-OXDANT	Col_r 178.5 I[b]	I 153.5 (0.87) Col_r[a]	228
14-OXDANT	Col_r 87.3 (0.01) Col_o 177.0 (4.26) I[a]	I 151.7 (2.62) Col_o 97.2 (0.09) Col_r[a]	246

[a] Transition temperatures (peak, in °C) and associated enthalpy changes in brackets in kJ mol^{-1} obtained from DSC. [b] Transition temperatures (in °C) obtained from POM. Abbreviations: Col_r = Columnar rectangular, Col_o = Columnar oblique, I = Isotropic liquid.

8) X-ray Scattering Studies:

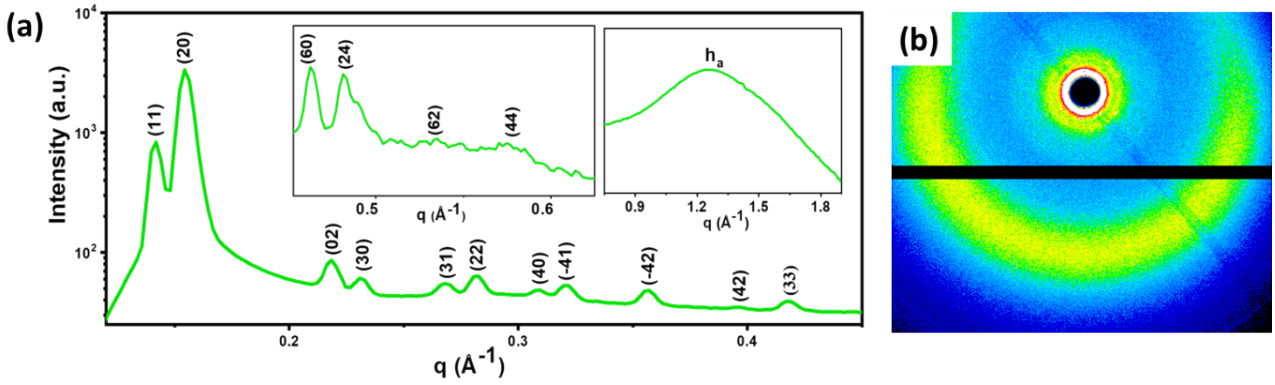

Fig. S13 (a) Small, mid (inset left) wide (inset right) angles X-ray scattering pattern of compound **14-OXDANT** at 150 °C (b) 2D pattern of the same.

Table S2: The observed and calculated *d*-spacings and corresponding reflecting planes of the diffraction peaks of the centered rectangular lattice observed at 30 °C for **10-OXDANT**.

The *d*-spacing is calculated by using the relation: $$d_{cal} = \frac{1}{\sqrt{\frac{h^2}{a^2} + \frac{k^2}{b^2}}}$$, where *h*, *k* are the Miller indices with *h* + *k* = *even* and *a* & *b* are the lattice parameters. The lattice parameters are *a* = 74.44Å, *b* = 52.63Å.

(hk)	***d-spacing Experimental d_{obs} (Å)***	***d-spacing Calculated d_{cal} (Å)***	***Relative Intensity I(hk)***	***Multiplicity***	***Phase Φ(hkl)***
1 1	42.97	42.97	100.00	4	0
2 0	37.22	37.22	23.88	2	0
0 2	26.45	26.32	3.87	2	0
2 2	21.58	21.49	6.50	4	π
4 0	18.52	18.61	3.58	2	0
1 3	17.17	17.08	3.25	4	0
4 2	15.17	15.19	//	//	//
3 3	14.25	14.32	2.37	4	0
0 4	13.34	13.16	2.08	2	0
6 0	12.42	12.41	1.79	2	0
5 3	11.32	11.35	//	//	//
4 4	10.64	10.74	//	//	//
4 6	8.04	7.93	//	//	//
8 4	7.59	7.60	//	//	//
$\mathbf{h_a}$	4.76	Fluid alkyl chain			
$\mathbf{h_{ac}}$	4.41	Partially crystalized alkyl chain			
$\mathbf{h_c}$	3.86	л-л interaction			

Table S3: The observed and calculated *d*-spacings and corresponding reflecting planes of the diffraction peaks of the centered rectangular lattice observed at 30°C for **12-OXDANT**. The *d*-spacing is calculated by using the relation: $d_{cal} = \frac{1}{\sqrt{\frac{h^2}{a^2} + \frac{k^2}{b^2}}}$, where *h*, *k* are the Miller indices with *h* + *k* = *even* and *a* & *b* are the lattice parameters. The lattice parameters are *a* = 79.78Å, *b* = 55.75Å.

(hk)	***d-spacing Experimental d_{obs} (Å)***	***d-spacing Calculated d_{cal} (Å)***	***Relative Intensity I(hk)***	***Multiplicity***	***Phase Φ(hkl)***
1 1	45.70	45.70	100.00	4	0
2 0	39.89	39.89	32.85	2	0
0 2	28.01	27.88	3.32	2	0
2 2	22.96	22.85	4.25	4	π
4 0	19.83	19.94	2.60	2	0
1 3	18.23	18.10	2.31	4	0
4 2	16.21	16.22	//	//	//
3 3	15.21	15.23	1.80	4	0
0 4	14.09	13.94	1.62	2	0
6 0	13.26	13.30	1.56	2	0
6 2	12.02	12.00	//	//	//
4 4	11.24	11.42	//	//	//
4 6	8.63	8.42	//	//	//
8 4	8.05	8.11	//	//	//
$\mathbf{h_a}$	4.82	Fluid alkyl chain			
$\mathbf{h_{ac}}$	4.41	Partially crystalize alkyl chain			
$\mathbf{h_c}$	3.87	л-л interaction			

Table S4: The observed and calculated *d*-spacings and corresponding reflecting planes of the diffraction peaks of the centered rectangular lattice observed at 30°C for **14-OXDANT**. The *d*-spacing is calculated by using the relation: $d_{cal} = \frac{1}{\sqrt{\frac{h^2}{a^2} + \frac{k^2}{b^2}}}$, where *h*, *k* are the Miller indices with *h* + *k* = *even* and *a* & *b* are the lattice parameters. The lattice parameters are *a* = 79.38Å, *b* = 54.87Å.

(hk)	***d-spacing Experimental d_{obs} (Å)***	***d-spacing Calculated d_{cal} (Å)***	***Relative Intensity I(hk)***	***Multiplicity***	***Phase Φ(hkl)***
1 1	45.14	45.14	100.00	4	0
0 2	27.44	27.44	3.67	2	π
2 2	22.62	22.57	3.36	4	π
4 0	19.93	19.84	2.90	2	0
1 3	17.80	17.82	2.67	4	0
4 2	15.95	16.08	2.37	4	0
0 4	13.61	13.72	2.44	2	0
$\mathbf{h_a}$	4.78	Fluid alkyl chain			
$\mathbf{h_{ac}}$	4.41	Partially crystalize alkyl chain			
$\mathbf{h_c}$	3.82	л-л interaction			

Table S5: The observed and calculated *d*-spacings and corresponding reflecting planes of the diffraction peaks of the oblique lattice observed at 150°C for the compound **14-OXDANT**. The *d*-spacing is calculated by using the relation: $$d_{cal} = \frac{sin(\alpha)}{\sqrt{\frac{h^2}{a^2} + \frac{k^2}{b^2} - \frac{2h\,k\,cos(\alpha)}{a\,b}}}$$, where *h*, *k* are the Miller indices and *a*, *b* & *α* are the lattice parameters. The lattice parameters are *a* = 81.51Å, *b* = 57.52Å & α = 94.85.

(hk)	***d-spacing Experimental d_{obs} (Å)***	***d-spacing Calculated d_{cal} (Å)***	***Relative Intensity I(hk)***	***Multiplicity***
1 1	45.07	45.07	24.94	2
2 0	40.61	40.61	100.00	2
0 2	28.66	28.66	2.57	2
3 0	27.07	27.07	1.79	2
3 1	23.61	23.72	1.65	2
2 2	22.40	22.53	1.88	2
4 0	20.31	20.30	1.44	2
-4 1	19.52	19.67	1.58	2
-4 2	17.57	17.27	1.43	2
4 2	15.93	15.94	1.02	2
3 3	15.06	15.02	1.17	2
6 0	13.58	13.54	1.12	2
2 4	13.06	13.17	1.11	2
6 2	11.74	11.86	//	//
4 4	10.98	11.27	//	//

$\mathbf{h_a}$	4.97	Fluid alkyl chain

9) Photophysical Studies:

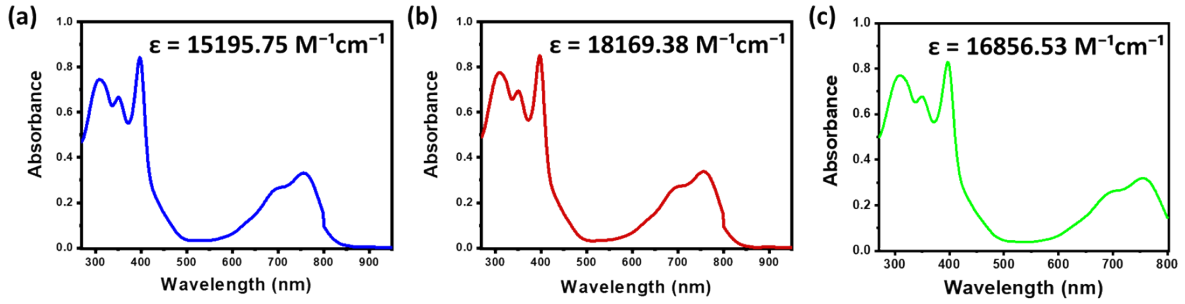

Fig. S14 Absorption spectra of (a) **10-OXDANT**, (b) **12-OXDANT** and (c) **14-OXDANT** in chloroform solvent of 10^{-5} M concentration, with their corresponding molar extinction coefficients (ε).

10) Electrochemical Studies:

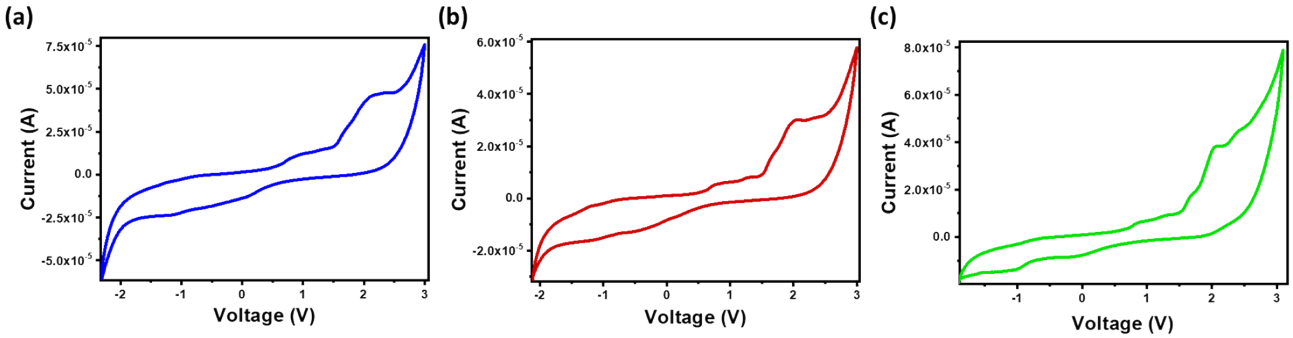

Fig. S15 Cyclic voltammogram of compound (a) **10-OXDANT,** (b) **12-OXDANT** and (c) **14-OXDANT** HPLC dichloromethane solution of tetrabutylammonium hexafluorophosphate (0.1 M) at a scanning rate 50 mVs^{-1} (Experimental conditions: $Ag/AgNO_3$ as reference electrode, platinum wire as counter electrode, glassy carbon as working electrode, tetrabutylammonium hexafluorophosphate (0.1 M) as supporting electrolyte, room temperature).

11) Computational Studies:

To understand the electronic properties and frontier molecular orbital energy levels of **OXDANT** DLCs, **10-OXDANT** was taken as the representative compound. Theoretical calculations were carried out with the Gaussian 09 suite of packages.[2] A full optimization was carried out using the hybrid functional, Becke's three parameter exchange and the LYP Correlation Functional (B3LYP)[3] at a split valence basis set 6-31G(d,p).

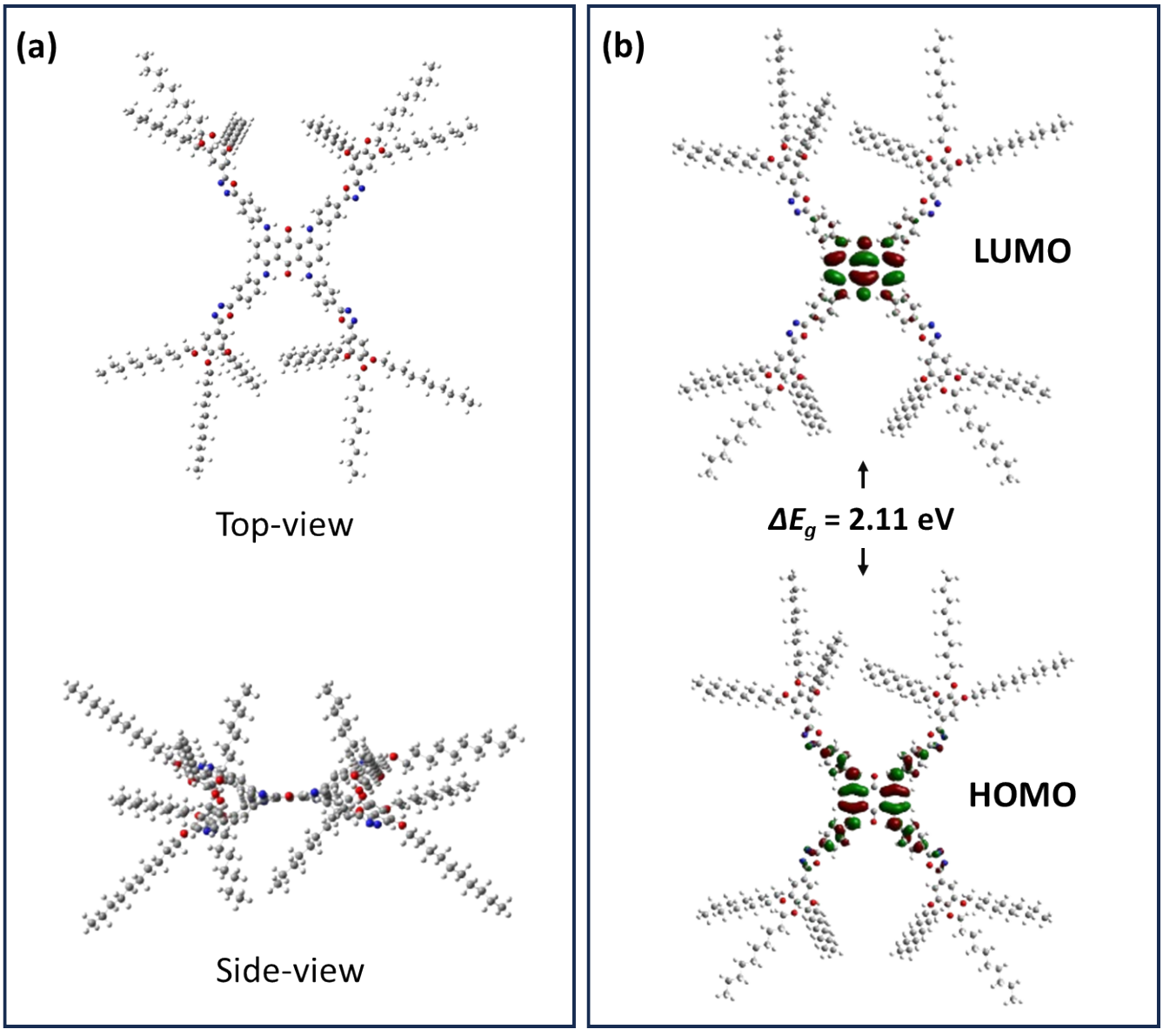

Fig. S16 Optimized geometry and electronic distribution of frontier molecular orbitals (HOMO and LUMO) of the representative compound **10-OXDANT**.

12) Nanofilm and charge transport studies:

The hole-only devices were prepared in an identical procedure as reported by us previously,[4] which is re-iterated below for **OXDANT**, along with fabrication procedure of electron-only devices.

ITO/PEDOT:PSS/**OXDANT**/MoO_3/Ag was employed to fabricate the hole-only devices. The ITO-coated glass substrates were cleaned successively by sonication in detergent water, deionized water, acetone, and isopropanol for 20 min at each step. Clean substrates were kept in vacuum oven, followed by 20 minutes of UV-ozone treatment before spin-coating. The treated substrates were spin-coated with PEDOT:PSS solution under 3000 rpm for 40 s, and annealed at 155 °C for 10 minutes. The active layer **OXDANT** solution was prepared in chloroform at a total concentration of 10 mg/ml. It was spin-coated on top of the PEDOT:PSS layer inside a glove box for the hole-only devices. The spin speed was standardized at 3000 rpm for 50s to obtain uniform active layer film with desired thickness. Then substrates were transferred to thermal evaporation system, after which 10 nm MoO_3 layer and 100 nm silver (Ag) top metal electrode were deposited successively on top of active layer under a pressure of 2×10^{-6} torr. Similarly for the electron-only devices, **OXDANT** solution was spin-coated on ZnO layer, and Ag was directly deposited on it. The active device area (A) was defined to be 0.09 cm^2 by using a shadow mask and the thickness (l) for the films was measured to be ~100 nm using a profilometer. Calculated dielectric constants for **10-OXDANT**, **12-OXDANT** and **14-OXDANT** were 6.50, 6.44 and 4.03, respectively.

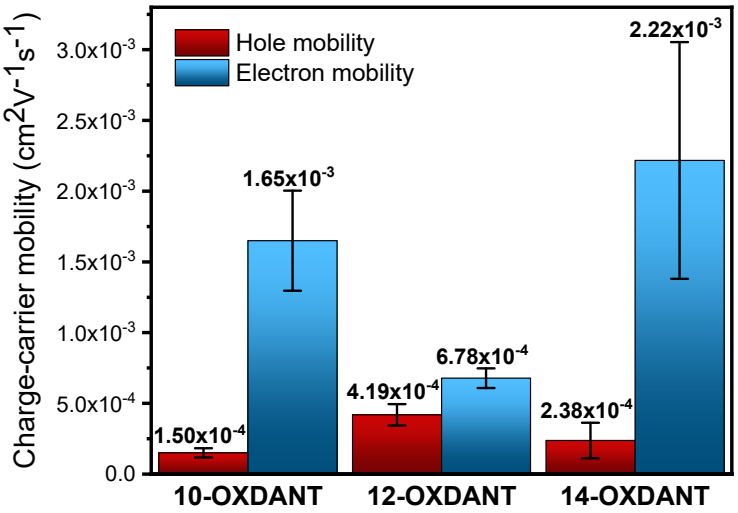

Fig. S17 Statistical charge-carrier mobility data for the **OXDANT** DLCs.

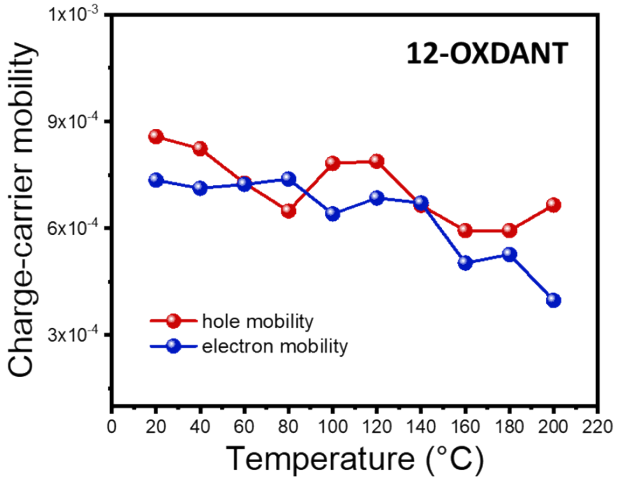

Fig. S18 Hole and electron mobilities of **12-OXDANT** with varying temperature.

Fig. S18 demonstrates very weak temperature dependence for both hole and electron mobilities, suggesting dominant electronic charge-transport and negligible contributions from thermally activated protonic or ionic pathways.

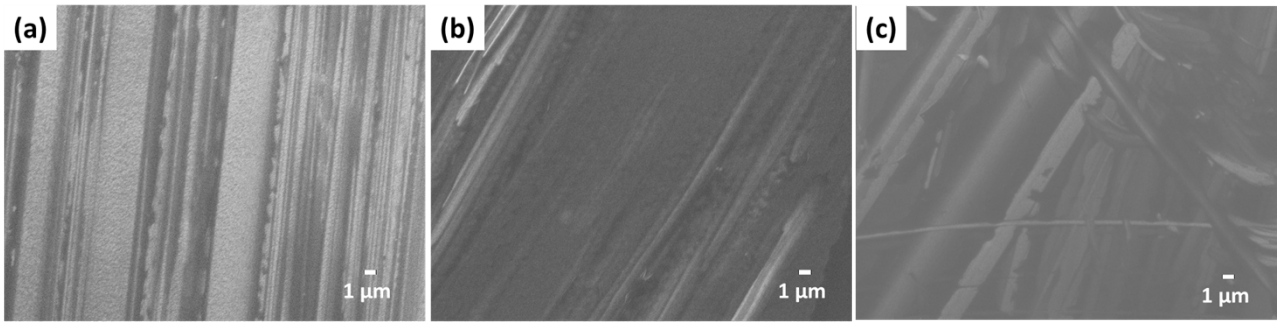

Fig. S19 SEM images of (a) **10-OXDANT,** (b) **12-OXDANT** and (c) **14-OXDANT** nanofilms spin-coated on ITO-coated glass.

13) References:

1. R. De, J. De, S. P. Gupta, I. Bala, Ankita, Tarun, U. K. Pandey and S. K. Pal, *Journal of Materials Chemistry C*, 2023, **11**, 980-985.
2. M. Frisch, *Inc, Wallingford CT*, 2009, **201**.
3. A. D. Becke, *The Journal of chemical physics*, 1993, **98**, 5648-5652.
4. R. De, M. Maity, A. Joseph, S. P. Gupta, Y. Nailwal, M. A. Namboothiry and S. K. Pal, *Small*, 2024, **20**, 2308983.